

Ultrafast formation of domain walls of a charge density wave in SmTe₃

M. Trigo,^{1,2,*} P. Giraldo-Gallo,^{3,4} J. N. Clark,¹ M. E. Kozina,^{1,2,3} T. Henighan,^{1,2,5} M. P. Jiang,^{1,2,5} M. Chollet,⁶ I. R. Fisher,^{2,3} J. M. Glowina,⁶ T. Katayama,⁷ P. S. Kirchmann,² D. Leuenberger,^{2,3} H. Liu,^{1,5} D. A. Reis,^{1,2,3} Z. X. Shen,^{2,3} and D. Zhu⁶

¹Stanford PULSE Institute, SLAC National Accelerator Laboratory, Menlo Park, California 94025, USA

²Stanford Institute for Materials and Energy Sciences, SLAC National Accelerator Laboratory, Menlo Park, California 94025, USA

³Department of Applied Physics, Stanford University, Stanford, California 94305, USA

⁴Department of Physics, Universidad de Los Andes, Bogotá 111711, Colombia

⁵Department of Physics, Stanford University, Stanford, California 94305, USA

⁶Linac Coherent Light Source, SLAC National Accelerator Laboratory, Menlo Park, California 94025, USA

⁷Japan Synchrotron Radiation Research Institute, 1-1-1 Kouto, Sayo-cho, Sayo-gun, Hyogo 679-5198, Japan



(Received 16 June 2020; revised 14 January 2021; accepted 21 January 2021; published 15 February 2021)

We study ultrafast x-ray diffraction on the charge density wave (CDW) of SmTe₃ using an x-ray free-electron laser. The high momentum and time resolution afforded by the x-ray laser enabled capturing fine wave-vector and time-dependent features of the CDW that originate from fast (in time) and sharp (in real space) variations of the CDW lattice distortion, which we attribute to an inversion of the order parameter. These domain inversions occur near the surface and are caused by the short penetration depth of the near-infrared pump with the wavelength centered at 800 nm, resulting in CDW domain walls perpendicular to the sample surface. These domain walls break the CDW long-range order on the scale of the x-ray probe depth, controlled experimentally by the x-ray incidence angle and suppress the diffraction intensity of the CDW for times much longer than the ~ 1 -ps recovery of the electronic gap observed in time and angle-resolved photoemission spectroscopy. We model the spatial and temporal dependences of the order parameter using a simple Ginzburg-Landau model with all the parameters obtained from the published literature. We find reasonable agreement between the calculated and the measured diffraction across the momentum, time, fluence, and incidence angle dependence without adjusting any parameters. We reconstruct the spatial and temporal dependences of the lattice order parameter and find that at long times, depending on the pump fluence, multiple domain walls remain at distances of a few nanometers from the surface.

DOI: [10.1103/PhysRevB.103.054109](https://doi.org/10.1103/PhysRevB.103.054109)

A fast quench through a critical point produces topological defects separating domains with distinct values of the order parameter [1–3]. At much faster timescales, topological defects can be created in condensed-matter systems with a spontaneously broken symmetry by ultrafast laser pulses [4–6]. Fine control over these defects could provide a route to reach thermodynamically inaccessible [7–9] or topologically inequivalent states [10], enabling novel forms of control of quantum phases [11], but imaging the defects as they are produced by ultrafast pulses is a daunting challenge. Here we use high-resolution x-ray diffraction at the Linac Coherent Light Source (LCLS) x-ray free-electron laser facility (XFEL) to resolve fine momentum-dependent features in the dynamics of the charge density wave (CDW) Bragg peak of SmTe₃ indicative of inhomogeneous variations in the CDW lattice distortion. We find that inhomogeneous photoexcitation due to the finite penetration depth of the femtosecond, near-IR pump flips the CDW amplitude at the surface, resulting in inequivalent regions separated by domain walls perpendicular to the sample normal. With the help of a simple model, we infer semiquantitatively the coherent evolution of the

spatially dependent order parameter. The fine time resolution allows us to observe the production and stabilization of one–three domain walls, depending on the excitation fluence. The scattering from inequivalent domains result in destructive interference at the CDW diffraction, suppressing and broadening the Bragg peaks for up to nanoseconds [12], even though the electronic order measured by time and angle-resolved photoemission spectroscopy (trARPES) establishes much earlier [5,13]. This result highlights the difference between surface and bulk probes and clarifies the origin of the surprisingly large discrepancy in the recovery timescales observed by diffraction [5,14,15] and time-resolved photoemission spectroscopy [5,13,16,17].

We focus on the CDW in SmTe₃ with ordering wave-vector $(0, 0, q)$ reciprocal lattice units with $q \approx 2/7$ [see the structure in Fig. 1(a)], which develops at $T < T_c = 416$ K. The RTe₃ (R is a rare-earth ion) class of layered materials has recently attracted attention as a model system to investigate the dynamics of symmetry-breaking phase transitions [4,5,9,12,14,15]. An intriguing puzzle of their ultrafast dynamics is the large discrepancy between the recovery of the electronic CDW gap observed in trARPES on the order of 1 ps [5,13,16,17], and the recovery of the CDW diffraction peaks [5,14,15] on the order of nanoseconds [12]. The interpretation

*Corresponding author: mtrigo@slac.stanford.edu

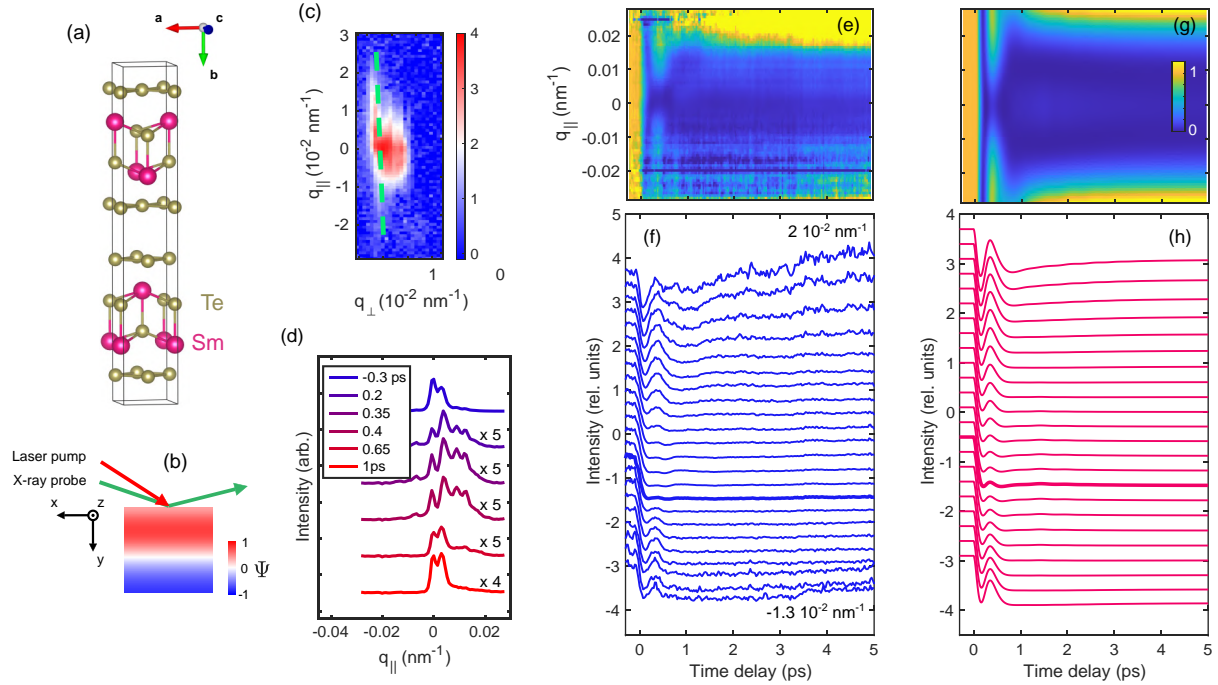


FIG. 1. (a) The crystal structure of SmTe_3 without the CDW distortion. (b) Geometry of the experiment and a representative snapshot of the inhomogeneous CDW distortion $\Psi(y, t)$ (see the text for details). (c) Detector image (\log_{10} intensity scale) of the $(2, 2, 1 - q)$ CDW peak at room temperature taken at a grazing incidence angle of $\alpha = 0.3^\circ$. We define $\mathbf{q}_{\parallel} = (0, q_{\parallel}, 0)$ parallel to the sample normal (b axis) and $\mathbf{q}_{\perp} = q_{\perp}(0.75, 0, 0.66)$ on the plane of the sample surface. (d) Profiles of the peak for representative delays along the dashed green line in (c) for the incident fluence of $1 \text{ mJ}/\text{cm}^2$. (e) Contour plot of $\tilde{S}(q_{\parallel}, t)$ defined in the text at wave vectors marked by the dashed line in (c). (f) Individual traces of (e) evenly spaced between $q_{\parallel} = -0.013 \text{ nm}^{-1}$ (bottom trace) and $q_{\parallel} = 0.02 \text{ nm}^{-1}$ (top trace), displaced vertically for clarity. (g) and (h) Calculated $\tilde{S}(q_{\parallel}, t)$ from the model in the text at the same wave vectors as in (e) and (f), respectively, for $\eta = 2$. The traces for $q_{\parallel} = 0$ in (f) and (h) are indicated with a thicker line.

given in Ref. [5] is that the amplitude of the CDW recovers in ~ 1 ps but the long-range order probed by diffraction is destroyed by phase modes. Our observations are consistent with this interpretation, but the initial loss of Bragg intensity is due to the inversion of the CDW amplitude (a π phase shift) near the sample surface, produced by the strong inhomogeneous absorption of the pump pulse [4]. We emphasize that such a discrepancy between the CDW order at the surface probed by trARPES and the CDW order in the bulk probed by diffraction [5] is not unique to this material system [18], suggesting that the ultrafast dynamics of CDW orders in strongly optically absorbing materials may, in general, be more subtle than an average “melting” of a CDW order into the high-symmetry phase. Clearly, better visualization of how these defects are created and decay will clarify their topological stability and will yield new insight into how they stabilize other degrees of freedom [9,19,20].

Room-temperature experiments using 9.5-keV x-ray pulses were carried out at the x-ray pump-probe station at the LCLS [21]. Grazing incidence diffraction [Fig. 1(b)] with $0.3 < \alpha < 0.5^\circ$, where α is the angle between the incident x-ray beam and the sample surface, was used to limit the x-ray penetration depth to $y_0 < 50 \text{ nm}$. (see the additional details in the Supplemental Material [22] and in Ref. [14]).

Figure 1(c) shows a static image of the $(2, 2, 1 - q)$ CDW sideband (\log_{10} scale). This CDW peak is mostly in plane, the vertical direction on the image is nearly along the b axis,

thus, we define $\mathbf{q}_{\parallel} = (0, q_{\parallel}, 0)$, the relative wave-vector offset from the nominal $(2, 2, 1 - q)$ reflection. Similarly, the horizontal detector direction relative to the nominal $(2, 2, 1 - q)$ reflection is $\mathbf{q}_{\perp} = q_{\perp}(0.75, 0, 0.66)$. The peak is elongated in the b direction even before the pump strikes, a signature that the correlation length along the b axis is shorter than on the a - c plane [23]. Figure 1(d) shows the q_{\parallel} dependence of the peak for representative delays at wave vectors along the widest part of the peak, indicated by the dashed line in Fig. 1(c). There is a slight shift in the peak in q_{\perp} , either due to a change in magnitude or the direction of the wave vector [24] (see the Supplemental Material [22]). The incident excitation fluence for these data was $1 \text{ mJ}/\text{cm}^2$ [14]. The fine structure of the peaks in Fig. 1(d) is likely due to preexisting domains deep beneath the surface, which do not seem affected by the pump. Since the total intensity is almost completely suppressed by the pump, the traces for $t > 0$ are scaled as indicated in the figure to increase visibility. Figure 1(d) shows changes to the peak shape as well as intensity, particularly, between $0 < t < 0.4$ ps, which seems to recover at $t > 0.65$ ps albeit with a much lower intensity [see the scaling factors in Fig. 1(d)]. To better visualize the dynamics we normalize the \mathbf{q}_{\parallel} profiles to the average at $t < -0.1$ ps (indistinguishable from the unpumped profile). In Fig. 1(e) we show a color intensity plot of the normalized structure factor $\tilde{S}(q_{\parallel}, t) = S(q_{\parallel}, t)/S(q_{\parallel}, t < 0)$ for the same wave vectors as in (d), and in Fig. 1(f) we plot representative intensity-vs-time traces of

the same data. The normalization of $\tilde{S}(q_{\parallel}, t)$ removes the static modulation of the peak and brings out the time-dependent changes as can clearly be seen in (e) and (f). At $t \approx 0$ ps the intensity is almost completely suppressed followed by a peak in $\tilde{S}(q_{\parallel}, t)$ at $t = 0.4$ ps for wave-vectors $|q_{\parallel}| > 0.005 \text{ nm}^{-1}$ and a slow increase in the intensity for these wave vectors at later times. Since \tilde{S} is normalized, this indicates a sudden increase in the width of the diffraction peak at ~ 0.4 ps that partially relaxes back and changes slowly after $t > 0.5$ ps. This broadening of the peak is a signature of inhomogeneous dynamics in the CDW lattice distortion. Furthermore, the two dips where $\tilde{S} \approx 0$ at ~ 0.2 and 0.5 ps in the time traces in Figs. 1(e) and 1(f) are points where the CDW amplitude vanishes (averaged over the probe volume), whereas the sharp bump at 0.3 ps appears because the CDW amplitude flips sign. Similar observations of an overshoot of the order parameter were made in Refs. [14,25]. All these taken together indicate that the order parameter must have one or more phase flips along the y direction after ~ 1 ps.

To illustrate the creation of domain walls and their signatures in the diffraction intensity, we consider a minimal one-dimensional model with a real-valued order parameter $\Psi(y, t)$, which represents the CDW lattice distortion in SmTe_3 . Although phase fluctuations are expected in this incommensurate CDW, they take time to develop and do not affect the initial dynamics. Here, y is the direction perpendicular to the sample surface as shown schematically in Figs. 1(a) and 1(b). A π phase shift in Ψ represents a reversal of the amplitude of the CDW distortion propagating along the y axis [Figs. 1(a) and 1(b)]. We consider a spatially and temporally dependent Ginzburg-Landau potential [4,25,26],

$$V(\Psi) = r(y, t)|\Psi|^2 + \frac{1}{2}|\Psi|^4 + \xi^2|\nabla\Psi|^2, \quad (1)$$

where the third term accounts for the strain energy of a spatially inhomogeneous configuration [27]. Here $r = -1$ and $\Psi = \pm 1$ ($r > 0$ and $\Psi = 0$) correspond to the CDW ordered (disordered) phase, and $\xi = 1.2$ nm is the coherence length [4]. The coefficient $r(y, t > 0) = \eta e^{-t/\tau} e^{-y/y_p} - 1$ represents the sudden photoexcitation on the potential energy with $\tau = 1$ ps and η proportional to the pump fluence [4,14,25]. Importantly, $r(y, t)$ is spatially inhomogeneous due to the finite penetration depth of the pump $y_p = 20$ nm. As we will show next, for sufficiently high excitation, $r > 0$ near the surface and Ψ can transiently be reversed producing alternating regions with $\Psi = \pm 1$ [Fig. 2(a)]. When the electronic excitation recovers quickly, i.e., when τ is fast compared with the dynamics, the inhomogeneities in Ψ are frozen leaving behind domain walls.

We integrate the equation of motion derived from the potential in Eq. (1) numerically, see the Supplemental Material [22]. Figure 2(a) shows $\Psi(y, t)$ (blue curve, right axis) and $r(y, t)$ (red curve, left axis) at representative times for $\eta = 2$ (see the Supplemental Material movies [22]). Figure 2(b) shows the potential $V(y, t)$ for two representative depths $y = 0$ (purple curve) and $y = 13$ nm (green curve). Initially, $r(y = 0, t = 0) = 1$, and the potential is strongly harmonic at $y = 0$ [purple line in (b)], and $\Psi(y = 0, t)$ acquires significant potential energy (purple dot). On the other hand, at $y = 13$ nm, $r \approx 0$, the potential is mostly quartic (green curve),

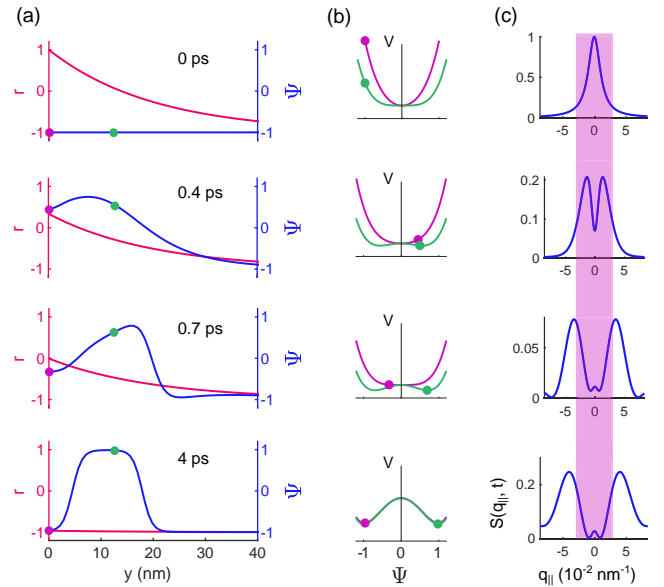


FIG. 2. (a) snapshots of $\Psi(y, t)$ (blue) and the quadratic coefficient $r(y, t)$ (red). (b) Solid lines show $V[\Psi(y, t)]$ and the corresponding value of $\Psi(y, t)$ at delays shown in (a) for $y = 0$ (purple dot) and $y = 13$ nm (green dot), also indicated in (a). (c) Structure factor $S(q_{\parallel}, t)$ produced by the corresponding $\Psi(y, t)$ shown in (a). q_{\parallel} is the wave vector parallel to y with $q_{\parallel} = 0$ as the nominal CDW Bragg condition. The shaded area indicates the range of wave vectors probed in the experiment.

and Ψ has less potential energy (green dot). At $t = 0.4$ ps the order parameter has reversed from the initial $\Psi = -1$ to $\Psi > 0$ for $y \lesssim 20$ nm, whereas the potential is recovering towards the initial double well with $r = -1$ (a). At $t = 0.4$ ps the potential at $y = 13$ nm has recovered the double-well structure [green curve in Fig. 2(b)], and Ψ does not have sufficient kinetic energy to cross the barrier back to the negative side. In contrast, the potential near the surface has not developed the double-well structure yet (purple trace at $t = 0.4$ ps), and Ψ has enough energy to complete a second flip back to the $\Psi = -1$ side. At $t = 0.7$ ps the double well starts to develop also at the surface, eventually freezing the order parameter on the $\Psi = -1$ side at the surface. Finally at $t = 4$ ps, $r = -1$ everywhere, and Ψ freezes with two domain walls. The number of final domain walls depends on the initial strength of the excitation η . As shown here, $\eta \approx 2$ produces two domain walls; for $\eta \approx 1$ only one domain wall forms, and for $\eta < 1$ no defects form since $r < 0$ everywhere in this case. Finally, the observed diffraction intensity is proportional to the CDW structure factor,

$$S(q_{\parallel}, t) = \left| \int_0^{\infty} \Psi(y, t) e^{-y/y_0} e^{iq_{\parallel}y} dy \right|^2, \quad (2)$$

where q_{\parallel} is the wave vector along y and y_0 is the x-ray penetration depth at grazing incidence [22]. Figure 2(c) shows a drastic decrease in $S(q_{\parallel}, t)$ at the nominal CDW Bragg condition, $q_{\parallel} = 0$, but it also broadens suddenly at 0.4 ps, demonstrated by the strong shoulders away from $q_{\parallel} = 0$. Although the peak shape recovers slightly, it remains distorted and suppressed at times $t > 4$ ps.

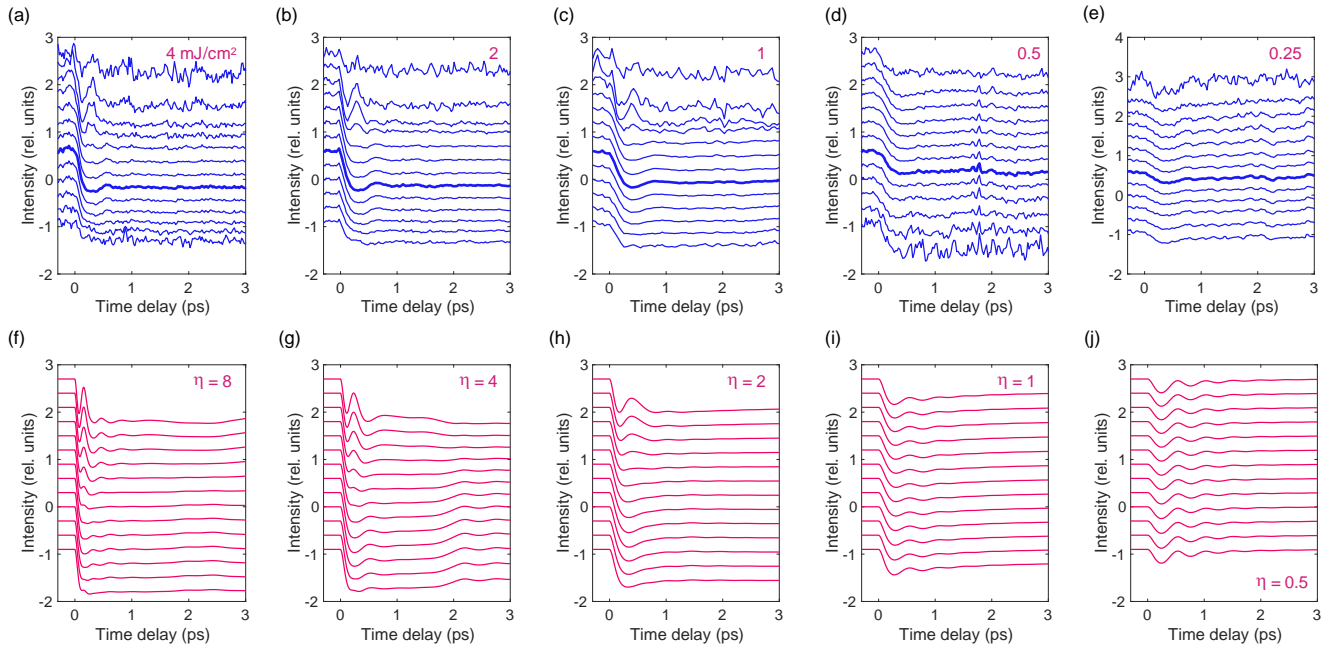


FIG. 3. (a)–(e) Dynamics of the $(1, 7, q)$ peak at incident fluences of 4, 2, 1, 0.5, and 0.25 mJ/cm^2 . (f)–(j) Simulation of $\tilde{S}(q_{\parallel}, t)$ for $\eta = 8, 4, 2, 1$, and 0.5, corresponding to experimental panels (a)–(e), respectively. All the experimental traces were taken with an x-ray incidence angle of 0.5° . The wave vector for the nominal Bragg condition is indicated with a thick line, and the traces are separated by $1.49 \times 10^{-3} \text{ nm}^{-1}$ and have been displaced vertically for clarity. The spurious spike at 1.8 ps in (d) is due to a glitch in the x-ray source.

We use the one-dimensional model described above as qualitative guide to understand the features observed in $\tilde{S}(q_{\parallel}, t)$. Figures 1(g) and 1(h) show the simulated $\tilde{S}(q_{\parallel}, t)$ over the same wave vectors as in (e) and (f) with $y_0 = 14 \text{ nm}$ and $\eta = 2$ corresponding to an incident fluence of 1 mJ/cm^2 in the experiment [14,22]. The qualitative agreement is remarkable: a peak at wave-vectors $|q_{\parallel}| > 0.005 \text{ nm}^{-1}$ at $t \sim 0.4 \text{ ps}$ and later a slow gradual increase in the normalized intensity at high wave vectors. A few representative snapshots of $\Psi(y, t)$ are shown in Fig. 2(a) with the final configuration at $t = 4 \text{ ps}$ containing two domain walls at $y \sim 5$ and $y \sim 15 \text{ nm}$. Although domain walls are not topologically stable in an incommensurate CDW (they are destroyed by phase fluctuations), in SmTe_3 they seem fairly robust and exist for up to nanoseconds after the pump [12,15]. The suppression of the Bragg peak intensity in Fig. 1, a measure of the CDW long-range order, is a consequence of the destructive interference between the x rays scattered from domains with opposite signs of Ψ . This explains why the diffraction intensity is suppressed for much longer [12,14,15] than the recovery of the electronic order at the surface, which affects the measured CDW gap [5], the optical reflectivity [14,28], and the coefficient $r(y, t)$ in the potential energy. We emphasize that the domain walls lie at $y \sim 5$ and $y \sim 15 \text{ nm}$ and are likely to be present in ultrafast electron-diffraction experiments [5,9,12] on samples thicker than the optical penetration depth $y_p \sim 20 \text{ nm}$.

We now turn to the fluence dependence of $\tilde{S}(q_{\parallel}, t)$, summarized in Fig. 3 for (a)–(e) the $(1, 7, q)$ CDW peak measured at an incidence angle of $\alpha = 0.5^\circ$ and (f)–(j) the corresponding simulation. The traces correspond to wave vectors separated by $1.49 \times 10^{-3} \text{ nm}^{-1}$ along the vertical direction on the

detector and are displaced vertically for clarity. These wave vectors have a small projection on the a - c plane since $(1, 7, q)$ has a larger out-of-plane component. We find good qualitative agreement between the model and the experimental data. In particular, the peaks at $t < 0.5 \text{ ps}$ for the top traces away from the nominal Bragg condition are well reproduced over all the fluences $> 0.5 \text{ mJ}/\text{cm}^2$ (a)–(c) and (f)–(h). Importantly, this peak does not appear for fluences $\leq 0.5 \text{ mJ}/\text{cm}^2$ (d) and (e) which agrees with the simulation for $\eta \leq 1$ (i) and (j). For $\eta = 1$, $r(0, 0) = 0$, a regime associated with dynamical slowing down [29], thus, Ψ has a small kinetic energy and flips only once, producing a single domain wall. The overall intensity is suppressed by the domain wall, but there is no bump at 0.4 ps. Finally, no domain wall are produced for lower excitation $\eta < 1$ (e) and (j). In this case, the intensity recovers within a picosecond after a short nearly harmonic transient due to the coherent dynamics of the amplitude mode of the CDW [14,16,17,28,30,31].

The contour plots in Fig. 4 show the calculated dynamics of $\Psi(y, t)$ for (a)–(e) excitations of $\eta = 8, 4, 2, 1$ and 0.5 matching those of Fig. 3. Blue (red) corresponds to $\Psi < 0$ ($\Psi > 0$). For $\eta > 1$ the dynamics produces (d) one, (b) two, or (a) three domain walls, whose locations along the depth (vertical axis) depend on η . At $\eta = 0.5$ not only does $\Psi(y, t)$ not flip to $\Psi > 0$, but it behaves as a nearly harmonic oscillator whose frequency is slightly chirped with a longer period near the surface, which recovers to the equilibrium $\Psi = -1$ in less than 4 ps [Fig. 4(e)]. In the limit of small η , $\Psi(y, t)$ is harmonic around the initial potential minimum, and the dynamics of the CDW peaks reflect the coherent dynamics of the amplitude mode of the CDW [14]. Finally, for $\eta = 8$ and $\eta = 4$ [Figs. 4(a) and 4(b)], $r(0, t) > 0$

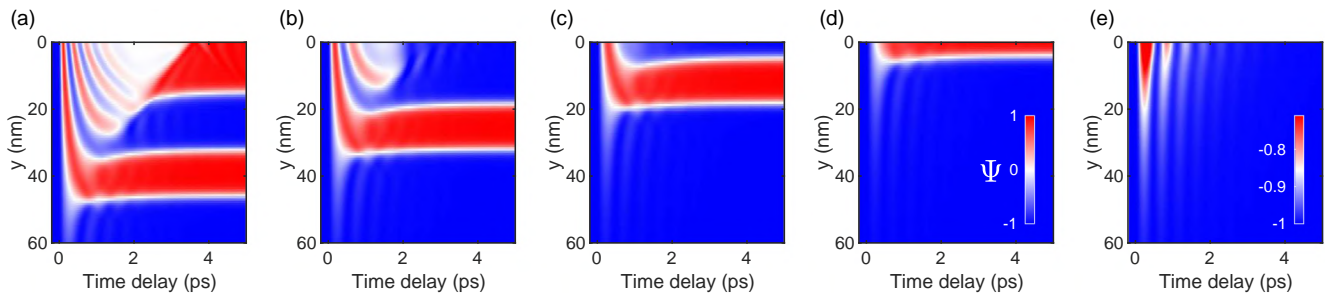


FIG. 4. (a)–(e) Contour plots of $\Psi(y, t)$ for $\eta = 8, 4, 2, 1$, and 0.5 , respectively. The color scale for (a)–(d) is shown in (d).

for $0 < t < 2$ ps and the potential at the surface $y = 0$ is quadratic for a sufficiently long time that $\Psi(y = 0, t)$ can perform several harmonic oscillations around the quadratic potential with $r(0, t) > 0$ (with the minimum at $\Psi = 0$) as can be seen in Figs. 4(a) and 4(b) near the surface ($y = 0$) and for $t < 2$ ps. This motion results in low-frequency oscillations in the diffraction data at $0 < t < 2$ ps, most clearly seen at $\alpha = 0.4^\circ$ [22].

Using ultrafast x-ray diffraction with a XFEL, we showed how photoexcitation generates nontrivial configurations of the order parameter in a charge ordered system in the form of domain walls propagating perpendicular to the sample surface. These domain walls break the CDW long-range order and suppress the diffraction intensity of the CDW for times much longer than the recovery of the electronic gap at the surface. These features are produced and measured stroboscopically over multiple repetitions of pump-probe pulses and must, therefore, be generated in a deterministic manner. This ability to produce defects on demand and to image their dynamics will provide a more complete picture of the competition

between the nearly degenerate c - and a -axis orders in $R\text{Te}_3$, which can be lifted by photoexcitation [9] and may pave the way towards better understanding of other coupled broken symmetries in the $R\text{Te}_3$ system [19] and other systems with competing orders [20,31].

Preliminary x-ray characterization was performed at BL7-2 at the Stanford Synchrotron Radiation Lightsource (SSRL). M.E.K., T.H., M.T., D.L., P.S.K., Z.X.S., P.G.-G., I.R.F., and D.A.R. were supported by the US Department of Energy, Office of Science, Office of Basic Energy Sciences through the Division of Materials Sciences and Engineering under Contract No. DE-AC02-76SF00515. Use of the LCLS and SSRL is supported by the US Department of Energy, Office of Science, Office of Basic Energy Sciences under Contract No. DE-AC02-76SF00515. J.N.C. was supported by the Volkswagen Foundation. Additional x-ray measurements were performed at BL3 of SACLAL with the approval of the Japan Synchrotron Radiation Research Institute (JASRI) (Proposal No. 2016A8008).

-
- [1] T. W. B. Kibble, *J. Phys. A* **9**, 1387 (1976).
 [2] W. H. Zurek, *Nature (London)* **317**, 505 (1985).
 [3] W. H. Zurek, *Phys. Rep.* **276**, 177 (1996).
 [4] R. Yusupov, T. Mertelj, V. V. Kabanov, S. Brazovskii, P. Kugar, J.-H. Chu, I. R. Fisher, and D. Mihailovic, *Nat. Phys.* **6**, 681 (2010).
 [5] A. Zong, A. Kogar, Y.-Q. Bie, T. Rohwer, C. Lee, E. Baldini, E. Ergeçen, M. B. Yilmaz, B. Freelon, E. J. Sie, H. Zhou, J. Straquadine, P. Walmsley, P. E. Dolgirev, A. V. Rozhkov, I. R. Fisher, P. Jarillo-Herrero, B. V. Fine, and N. Gedik, *Nat. Phys.* **15**, 27 (2019).
 [6] K. Nasu, *Photoinduced Phase Transitions* (World Scientific, Singapore, 2004).
 [7] L. Stojchevska, I. Vaskivskiy, T. Mertelj, P. Kugar, D. Svetin, S. Brazovskii, and D. Mihailovic, *Science* **344**, 177 (2014).
 [8] H. Ichikawa, S. Nozawa, T. Sato, A. Tomita, K. Ichiyangi, M. Chollet, L. Guerin, N. Dean, A. Cavalleri, S.-I. Adachi, T.-H. Arima, H. Sawa, Y. Ogimoto, M. Nakamura, R. Tamaki, K. Miyano, and S.-Y. Koshihara, *Nat. Mater.* **10**, 101 (2011).
 [9] A. Kogar, A. Zong, P. E. Dolgirev, X. Shen, J. Straquadine, Y.-Q. Bie, X. Wang, T. Rohwer, I.-C. Tung, Y. Yang, R. Li, J. Yang, S. Weathersby, S. Park, M. E. Kozina, E. J. Sie, H. Wen, P. Jarillo-Herrero, I. R. Fisher, X. Wang, and N. Gedik, *Nat. Phys.* **16**, 159 (2020).
 [10] E. J. Sie, C. M. Nyby, C. D. Pemmaraju, S. J. Park, X. Shen, J. Yang, M. C. Hoffmann, B. K. Ofori-Okai, R. Li, A. H. Reid, S. Weathersby, E. Mannebach, N. Finney, D. Rhodes, D. Chenet, A. Antony, L. Balicas, J. Hone, T. P. Devereaux, T. F. Heinz, X. Wang, and A. M. Lindenberg, *Nature (London)* **565**, 61 (2019).
 [11] D. N. Basov, R. D. Averitt, and D. Hsieh, *Nat. Mater.* **16**, 1077 (2017).
 [12] F. Zhou, J. Williams, S. Sun, C. D. Malliakas, M. G. Kanatzidis, A. F. Kemper, and C.-Y. Ruan, *Nat. Commun.* **12**, 566 (2021).
 [13] F. Schmitt, P. S. Kirchmann, U. Bovensiepen, R. G. Moore, J.-H. Chu, D. H. Lu, L. Rettig, M. Wolf, I. R. Fisher, and Z.-X. Shen, *New J. Phys.* **13**, 063022 (2011).
 [14] M. Trigo, P. Giraldo-Gallo, M. E. Kozina, T. Henighan, M. P. Jiang, H. Liu, J. N. Clark, M. Chollet, J. M. Glowia, D. Zhu, T. Katayama, D. Leuenberger, P. S. Kirchmann, I. R. Fisher, Z. X. Shen, and D. A. Reis, *Phys. Rev. B* **99**, 104111 (2019).
 [15] R. G. Moore, W. S. Lee, P. S. Kirchmann, Y. D. Chuang, A. F. Kemper, M. Trigo, L. Patthey, D. H. Lu, O. Krupin, M. Yi, D. A. Reis, D. Doering, P. Denes, W. F. Schlotter, J. J. Turner, G. Hays, P. Hering, T. Benson, J.-H. Chu, T. P. Devereaux, I. R. Fisher, Z. Hussain, and Z.-X. Shen, *Phys. Rev. B* **93**, 024304 (2016).
 [16] L. Rettig, J.-H. Chu, I. R. Fisher, U. Bovensiepen, and M. Wolf, *Faraday Discuss.* **171**, 299 (2014).

- [17] D. Leuenberger, J. A. Sobota, S.-L. Yang, A. F. Kemper, P. Giraldo-Gallo, R. G. Moore, I. R. Fisher, P. S. Kirchmann, T. P. Devereaux, and Z.-X. Shen, *Phys. Rev. B* **91**, 201106(R) (2015).
- [18] See for example in TaS₂, trARPES [32,33], diffraction [34]; in K_{0.3}MoO₃: trARPES [35], diffraction [25]; and in TiSe₂: trARPES [33,36], and diffraction [37].
- [19] J. J. Hamlin, D. A. Zocco, T. A. Sayles, M. B. Maple, J. H. Chu, and I. R. Fisher, *Phys. Rev. Lett.* **102**, 177002 (2009).
- [20] E. Fradkin, S. A. Kivelson, and J. M. Tranquada, *Rev. Mod. Phys.* **87**, 457 (2015).
- [21] M. Chollet, R. Alonso-Mori, M. Cammarata, D. Damiani, J. Defever, J. T. Delor, Y. Feng, J. M. Glownia, J. B. Langton, S. Nelson, K. Ramsey, A. Robert, M. Sikorski, S. Song, D. Stefanescu, V. Srinivasan, D. Zhu, H. T. Lemke, and D. M. Fritz, *J. Synchrotron Radiat.* **22**, 503 (2015).
- [22] See Supplemental Material at <https://link.aps.org/supplemental/10.1103/PhysRevB.103.054109> for additional data, simulation details, and movies.
- [23] N. Ru, C. L. Condron, G. Y. Margulis, K. Y. Shin, J. Laverock, S. B. Dugdale, M. F. Toney, and I. R. Fisher, *Phys. Rev. B* **77**, 035114 (2008).
- [24] D. Le Bolloc'h, A. A. Sinchenko, V. L. R. Jacques, L. Ortega, J. E. Lorenzo, G. A. Chahine, P. Lejay, and P. Monceau, *Phys. Rev. B* **93**, 165124 (2016).
- [25] T. Huber, S. O. Mariager, A. Ferrer, H. Schäfer, J. A. Johnson, S. Grübel, A. Lübecke, L. Huber, T. Kubacka, C. Dornes, C. Laulhe, S. Ravy, G. Ingold, P. Beaud, J. Demsar, and S. L. Johnson, *Phys. Rev. Lett.* **113**, 026401 (2014).
- [26] P. Kusar, T. Mertelj, V. V. Kabanov, J.-H. Chu, I. R. Fisher, H. Berger, L. Forró, and D. Mihailovic, *Phys. Rev. B* **83**, 035104 (2011).
- [27] W. L. McMillan, *Phys. Rev. B* **12**, 1187 (1975).
- [28] R. V. Yusupov, T. Mertelj, J.-H. Chu, I. R. Fisher, and D. Mihailovic, *Phys. Rev. Lett.* **101**, 246402 (2008).
- [29] A. Zong, P. E. Dolgirev, A. Kogar, E. Ergeçen, M. B. Yilmaz, Y.-Q. Bie, T. Rohwer, I.-C. Tung, J. Straquadine, X. Wang, Y. Yang, X. Shen, R. Li, J. Yang, S. Park, M. C. Hoffmann, B. K. Ofori-Okai, M. E. Kozina, H. Wen, X. Wang, I. R. Fisher, P. Jarillo-Herrero, and N. Gedik, *Phys. Rev. Lett.* **123**, 097601 (2019).
- [30] F. Schmitt, P. S. Kirchmann, U. Bovensiepen, R. G. Moore, L. Rettig, M. Krenz, J. H. Chu, N. Ru, L. Perfetti, D. H. Lu, M. Wolf, I. R. Fisher, and Z. X. Shen, *Science* **321**, 1649 (2008).
- [31] J. Chang, E. Blackburn, A. T. Holmes, N. B. Christensen, J. Larsen, J. Mesot, R. Liang, D. A. Bonn, W. N. Hardy, A. Watenphul, M. v. Zimmermann, E. M. Forgan, and S. M. Hayden, *Nat. Phys.* **8**, 871 (2012).
- [32] L. Perfetti, P. A. Loukakos, M. Lisowski, U. Bovensiepen, M. Wolf, H. Berger, S. Biermann, and A. Georges, *New J. Phys.* **10**, 053019 (2008).
- [33] S. Hellmann, T. Rohwer, M. Kalläne, K. Hanff, C. Sohr, A. Stange, A. Carr, M. M. Murnane, H. C. Kapteyn, L. Kipp, M. Bauer, and K. Rossnagel, *Nat. Commun.* **3**, 1069 (2012).
- [34] S. Vogelgesang, G. Storeck, J. G. Horstmann, T. Diekmann, M. Siviş, S. Schramm, K. Rossnagel, S. Schäfer, and C. Ropers, *Nat. Phys.* **14**, 184 (2018).
- [35] H. Y. Liu, I. Gierz, J. C. Petersen, S. Kaiser, A. Simoncig, A. L. Cavalieri, C. Cacho, I. C. E. Turcu, E. Springate, F. Frassetto, L. Poletto, S. S. Dhesi, Z.-A. Xu, T. Cuk, R. Merlin, and A. Cavalleri, *Phys. Rev. B* **88**, 045104 (2013).
- [36] C. Monney, M. Puppin, C. W. Nicholson, M. Hoesch, R. T. Chapman, E. Springate, H. Berger, A. Magrez, C. Cacho, R. Ernstorfer, and M. Wolf, *Phys. Rev. B* **94**, 165165 (2016).
- [37] E. Möhr-Vorobeva, S. L. Johnson, P. Beaud, U. Staub, R. De Souza, C. Milne, G. Ingold, J. Demsar, H. Schaefer, and A. Titov, *Phys. Rev. Lett.* **107**, 036403 (2011).